Fabrication and characterization of one- and two-dimensional regular patterns produced employing multiple exposure holographic lithography

A. JURKEVIČIŪTĖ[a], N. ARMAKAVIČIUS[a], D. VIRGANAVIČIUS[a], L. ŠIMATONIS[a], T. TAMULEVIČIUS[a,b*], S. TAMULEVIČIUS[a,b]
[a]*Kaunas University of Technology, Institute of Materials Science, K. Baršausko Str. 59, Kaunas, Lithuania, LT-51423*
[b]*Physics Department, Kaunas University of Technology, Studentų Str.50, Kaunas, Lithuania, LT-51368*

In this paper we describe fabrication and characterization methods of two-dimensional periodic microstructures in photoresist with pitch of 1.2 μm and lattice constant 1.2-4.8 μm, formed using two-beam multiple exposure holographic lithography technique. The regular structures were recorded employing different angular positions of the sample in between two and three sequential exposures, adding up fringes of various symmetries on thin positive tone photoresist layer spin-coated on floated glass substrates. After exposure and development, the resulting structures were analysed employing optical and scanning electron microscopy. It was demonstrated that structures with rhombus, triangular and square point lattice types with 2-fold, 4- fold or 6-fold rotational symmetry can be obtained. The results obtained from the micrographs were compared with the simulation results of interference field light intensity distribution. Camera images of the transmitted and diffracted laser beam light far field spatial distribution were compared with the fast Fourier transforms (FFT) of optical microscope dark field micrographs. Diffraction efficiency measurements were demonstrated as an efficient method to control quality of the structures as well as to optimize the multiple exposure processes.

(Received February 19, 2016; accepted April 6, 2017)

Keywords: Holographic lithography, Interference, Periodic structures, FFT, Diffraction patterns

1. Introduction

Interference or holographic lithography (HL) is emerging as very promising and powerful technique for creating structures with sub-micrometre to nanometre scale periodicities [1]. Currently fabrication of photonic crystals is perhaps the most common HL application [2]. Besides research trends in photonic crystals, HL is shown to be applicable in vast range of areas where regular microstructures are necessary. There have been shown successful attempts where formation of optical sensors [3-7], nanowires [8], porous membranes [9], broadband membrane reflectors [10], magnetic dots [11], nano-fluidic structures [12], micro lenses arrays [13], photonic phased arrays [14], polarization gratings [15] and, after introducing defects, optical channel drop filters [16] were performed employing HL.

HL technique is based on interference of two or more coherent laser beams and does not require photomasks like conventional contact lithography used in integrated circuit industry. Compared with other common lithography techniques including e-beam and nanoimprint used to produce arrays of nanometre sized features, HL can offer much higher throughput at a lower cost. Using shorter wavelengths (in EUV range) and immersion techniques, feature size approaching 10 nm were achieved [17, 18]. At the moment basically two instrumentation architectures are used for HL: the Lloyd's mirror interferometer, which is usually used for high resolution patterning and the dual beam interferometer which is used for large areas [19]. Despite the fact that HL is relatively easy to setup and operate, its main drawback is that it is limited only to patterning of periodic structures [10]. In its simplest form, when interference of two beams is imposed, such lithography is capable to produce 1D periodic structures, i.e. linear diffraction gratings. This limitation can be overcome by using multiple beams. For example, by using modified Lloyd's mirror interferometer into three-beam interferometer patterns with true hexagonal symmetry can be realised [20]. Applying four-beam HL setup and controlling the polarization and intensity threshold of the beam, two-dimensional periodic patterns can be created with a wide range of possible geometries [21, 22, 23]. Employing five and more beams complex quasi-periodic patterns can be produced [24, 25]. By using multiple beam interference combined with multi-photon polymerization technique, 3D microstructures can be fabricated [26].

On the other hand, 2D and 3D microstructures can also be achieved using two-beam multiple exposure HL process together with the sample rotation in between the individual exposures [1, 8-11, 13, 24, 27-40]. In such case, the resulting exposure dose of each individual exposure is accumulated as a sum of the partial exposures [28]. In this way various patterns can be created by changing number

of applied exposures and angle of the sample orientation [1]. Multiple two-beam HL exposure has been successfully realised employing Lloyd's mirror setup [19, 29-31, 41], and other optical systems including: mirrors in glazing incidence configuration [25], double-iris [27], beam-splitters [32, 38, 42]. The possibility to fabricate complex structures, including 3D patterns as well as production of hierarchical periodic patterns (with two different spatial periods) using a multiple exposure procedure was demonstrated in [39] and [40] correspondingly.

Two-beam multiple exposure interference technique possesses many advantages over the commonly used multi-beam interference technique, such as: simple optical setup, easy to fabricate different patterns by controlling the angle between sequential exposures and number of applied multiple exposures, and high contrast between the minimal and maximal intensities of interference fringes due to the identical polarization of two laser beams in the interference area. That is difficult to achieve using multi-beam interference method [27]. Recently areas as large as whole 4 inches (10 cm) wafer were reported to be patterned employing HL [43]. To obtain uniform patterns over large area, a laser with a long coherence length is required [1, 29].

In our previous research we have demonstrated that using two beam HL setup one is able to form diffraction gratings in photoresist [4] and later on, to transfer the pattern in DLC layer and use them as refractive index sensors to determine refractive index of liquids and track kinetics of chemical and biological processes [6, 7]. Moreover, we have shown that the sinusoidal relief imposed in the photoresist employing vacuum deposition and electrochemical processes can be replicated in polymer films for document optical security tag applications [44, 45].

In this paper we propose a systematic study where interference patterns in multiple exposure two beam HL system are simulated to produce complex 2D periodic structures. We demonstrate that the simulated interference fringes of variable geometry having rhombus, triangular and square point lattice types with 2-fold, 4-fold or 6-fold rotational symmetry can be produced experimentally after few seconds of exposure in a standard positive photoresist on glass substrates in several cm^2 area. Finally, we show that the diffraction patterns produced by these structures can be used for the fast quality control of the structures. As an example, different multiple exposure doses were examined to produce highest diffraction efficiency in the case of three exposures process.

2. Laser beam interference formalism

In order to calculate multiple exposure interference pattern intensity distribution at the sample surface, one has to consider two collimated laser beams interference formalism, i.e. to assume superposition of two monochromatic and linearly polarised waves and to use plane wave approximation. In this case electromagnetic waves can be described by complex wave functions [46]:

$$\mathbf{U}_1(\mathbf{r}_1,t)=\mathbf{p}_1E_1\exp\left(j\cdot(\omega_1 t+\mathbf{k}_1\mathbf{r}+\varphi_1)\right), \quad (1)$$

$$\mathbf{U}_2(\mathbf{r}_2,t)=\mathbf{p}_2E_2\exp\left(j\cdot(\omega_2 t+\mathbf{k}_2\mathbf{r}+\varphi_2)\right). \quad (2)$$

Here $\mathbf{p}_1$, $\mathbf{p}_2$ - polarization vectors, E_1, E_2 – electric field amplitudes, j – imaginary unit, ω_1, ω_2 – angular frequencies, t – time, $\mathbf{k}_1$, $\mathbf{k}_2$ – wave vectors ($\mathbf{k}=2\pi\hat{\mathbf{k}}/\lambda$), $\hat{\mathbf{k}}$ - unit vector presenting direction of phase velocity, $\lambda=\lambda_0/n$, λ_0 – free space wavelength, n – refractive index, $\mathbf{r}$ – position vector, φ_1, φ_2 – initial phases of the first and the second beam respectively. We can eliminate the first and the third terms in the exponent if we consider stationary case and do not evaluate initial phases. This can be done because in the case of two beams superposition, due to the difference of initial phases, the interference pattern is shifted, but its distribution remains unchanged. Since in the employed optical setup, described in Sec. 5.1, beam splitters produce two beams of nearly equal intensities, the electric field amplitudes E_1, E_2 are equal ($E_1=E_2$) so they can be denoted as E. Moreover, polarization terms can be removed from the equations, assuming that the produced beams have parallel polarization planes. Intensity resulting from two beams superposition is $I=\left|\mathbf{U}_1(\mathbf{r}_1)+\mathbf{U}_2(\mathbf{r}_2)\right|^2$. Using Eq. (1), (2) and assumptions described above, intensity distribution of the interference field produced by the superposition of two beams can be expressed as [46]:

$$I=2I+2I\cos\left(\mathbf{r}\cdot(\mathbf{k}_2-\mathbf{k}_1)\right). \quad (3)$$

This Equation shows that intensity of superposed beams at a certain point of space depends only on the phase difference of interfering beams $\left(\mathbf{r}\cdot(\mathbf{k}_2-\mathbf{k}_1)\right)$. Optical path R_i of each beam in polar coordinate system can be expressed as [33]:

$$R_i=\hat{\mathbf{k}}_i\cdot\mathbf{r}=x\cdot\sin(\theta_i)\cos(\phi_i)+y\cdot\sin(\theta_i)\sin(\phi_i)+z\cdot\cos(\theta_i) \quad (4)$$

here i – index indicating the beam number; θ – angle of incidence in the plane of incidence; ϕ – angle of beam projection in the plane perpendicular to the plane of incidence (see Fig. 1). Arrangement of the beams and angles used in Eq. (4) is depicted in Fig. 1. For the known wavelength and arrangement of the beams involved in the process, one can calculate intensity distribution pattern of the two beam interference field by using Eq. (3) and (4). In case of multi-exposure HL, intensity distribution can be calculated by summation of the interference fields created by each exposure:

$$I_{sum}=\sum_j I_j \quad . \quad (5)$$

Here j – number of exposures. Pitch of the interference fringes (Λ) of each exposure and accordingly pitch of the structures imposed in the photosensitive materials (for the fixed ϕ_i) depends on the angle of incidence θ_i, refractive

index of the medium surrounding the sample n and wavelength of the employed laser λ_0:

$$\Lambda = \frac{\lambda_0}{2n\sin\theta}, \tag{6}$$

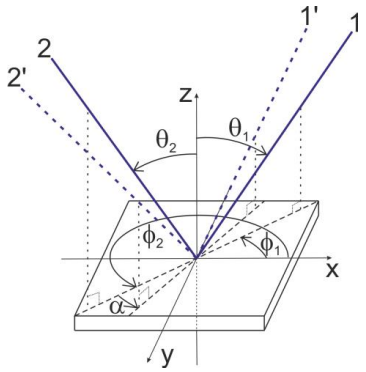

Fig. 1. Arrangement of two interfering beams with indicated notations used in Eq. (1)-(4). θ_1, θ_2 – angles between the incident beams (1, 2) and z axis in the plane of incidence. ϕ_1,ϕ_2 – angles between the incident beams projections in x-y plane and x axis. While 1' and 2' are beams in the second exposure with sample rotation by α angle in x-y plane around z axis between the sequential exposures

3. Simulation Results

Employing the developed formalism (Sec. 2) for the accumulated multiple two beam interference pattern exposure, the simulations of light intensity distributions for single exposure, two sequential exposures with different rotation angles α=15º-90º in x-y plane with steps of 15º and finally three exposures with two sequential rotations of α=60º were performed employing MATLAB (MathWorks) software. The simulated interference patterns are depicted in Fig. 2 and as it will be demonstrated in Sec. 5 they can be reproduced experimentally as corresponding surface relief structures after developing the exposed photosensitive material.

4. Experimental

4.1. Fabrication of the structures

The structures were patterned on 20 mm x 20 mm x 2 mm floated glass (Gravera) substrates. Glass substrates before the deposition of photoresist were cleaned employing RCA SC-1 cleaning method i.e. rinsing the substrates in H_2O+H_2O_2+NH_4OH (5:1:1) solution at 80 ºC for 10 minutes and washing off with deionised water. 100-200 µl per sample of ma-P 1205 positive tone photoresist (Micro resist technology) were used. Photoresist was spin-coated employing KW-4A spin-coater (Chemat technology). Spin-coating was performed at 500-700 rpm for 6 s and 3000-3200 rpm for 30 s. The thickness of a photoresist layer at ≥3000 rpm was 0.5 µm [47]. Photoresist was dried at 110 ºC for 30 s employing KW-4AH hot plate (Chemat technology). The exposure was performed using HeCd laser (λ=442 nm, 90 mW, CVI Melles Griot 4074-P-A03) in a custom made HL setup (see Fig. 3). The laser beam in the applied setup was expanded employing spatial filter, i.e. 40x, 0.65 NA microscope objective (Lomo) and 30 µm aperture (Standa), collimated with a 50 mm diameter and 75 mm focal length convex lens (Eksma Optics). The collimated beam was diffracted into two beams by the 50x50 mm 1800 l/mm diffraction grating beam splitter (Thorlabs). The diffracted beams were directed and overlapped on the sample holder with 50 mm diameter dielectric laser line mirrors (Eksma Optics). The sample on the rotatable sample holder was fixed with a vacuum chuck. Time of the exposure (4-9 s) was chosen depending on the laser power (89.7-90.8 mW) and corresponding applicable power density on the sample side (2.9-4.3 mW/cm^2).

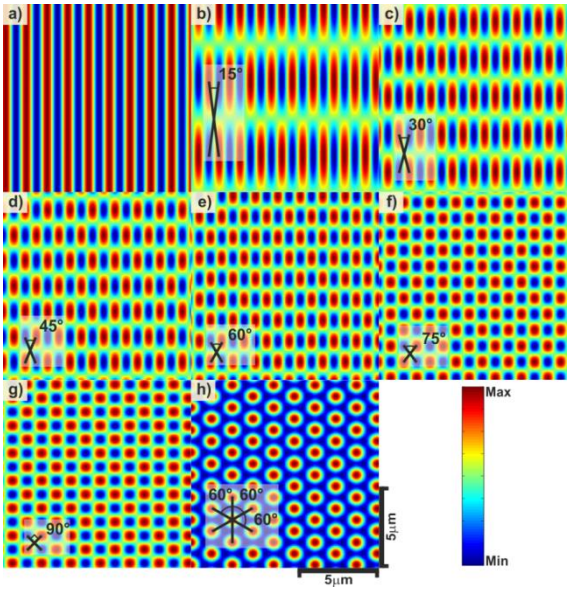

Fig. 2. Simulated 1D (a) and 2D (b-h) interference pattern intensity distributions employing different number of exposures and rotation angles between them (λ_0=442 nm, n=1, $\theta_{1,2}$=10º): a) single exposure, b) angle between two exposures α=15º, c) α=30º, d) α=45º, e) α=60º, f) α=75º, g) α=90º, h) angles between three exposures α_1=60º, α_2=120º. Lines and angles indicated in the images b-h represent resulting angles between the 2D lattice points in the accumulated interference pattern

1D periodic structures were fabricated by a single exposure. 2D periodic structures were fabricated by two or three exposures. Between the multiple exposures, the sample was rotated by an angle α (see Fig. 1). The angle α in the current rotatable sample holder can vary from 0º to 120º in 15º steps (see insets of Fig. 3). The incidence angles of two interfering beams were set to be identical θ_1=θ_2=θ 10±0.7º. Such angle provides pitch of the structure (see Eq. (5)) of 1.2 µm. The employed system is capable of producing sub-wavelength pitch [4-7], but in this case dimensions that are still visible on optical microscope were selected. The area of single exposure was

in the forms of an ellipse due to oblique incidence of the beams. The size of exposed area was limited by the size of the beam splitter and employed mirrors, i.e. 5 cm. After exposure the samples were developed in MF-26A developer (Micro resist technology) for 9-14 s. The details of the applied exposure are summarised in Table 1.

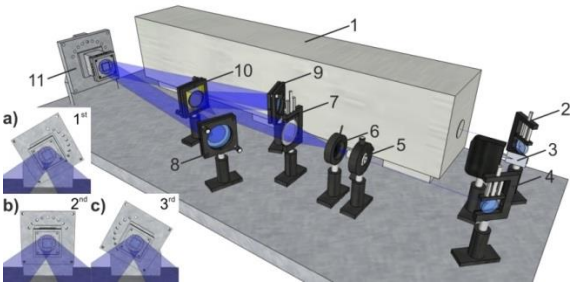

Fig. 3. Principle scheme of the employed two beam HL setup utilised for the multiple exposures. The system consists of mirrors - 2, 4, 8, 9, computer controlled shutter – 3, objective – 5, pinhole – 6, lens – 7, diffraction grating beam splitter – 10, rotatable sample holder – 11. The total path of a beam from the laser to the sample holder is approximately 232.5 cm. The insets depict snapshots of the sample holder positions for the three times exposed samples (Table 1, sample No. 8-11): a) initial position, b) second position (angle between exposures α_1=60 °), c) third position (α_2=120 °).

4.2. Analytical techniques

The fabricated structures were analysed employing optical microscope B-600MET (Optika) and scanning electron microscope (SEM) Quanta 200 FEG (FEI). Low vacuum mode enabling direct sample surface visualization without any further preparation was applied. Dark field optical microscope images of the fabricated structures were used to obtain frequency domain images of the periodic structures using 2D Fast Fourier Transforms (FFT) employing MATLAB (MathWorks) software. The experimental diffraction efficiency distributions for the produced periodic structures were obtained employing three different wavelength lasers: laser diode (Photonic products) λ=405 nm, diode pumped solid state laser (Apinex) λ=532 nm and HeNe laser (Melles Griot) λ=632.8 nm. The intensities of the diffracted light were measured using NOVA II power meter (Ophir) with PD200UV photodiode sensor. Far field diffraction pattern spatial distributions in the transmission regime obtained on a screen from the samples were registered with a compact digital camera (Power Shot A590, Canon).

Table 1. Applied exposure parameters of the HL setup for different samples: α – angle of rotations between exposures, θ – angle of incidence, t_e – duration of exposure, t_d – duration of development. Average laser power was 89.7 mW (88.6-90.8 mW), average power density at the sample 3.5 mW/cm^2 (2.9-4.3 mW/cm^2)

Sample No.	α (°)	θ (°)	t_e (s)	t_d (s)
1	-	10.3	7	14
2	15	10.3	7; 5	11
3	30	9	9; 6	10
4	45	10.3	7; 5	13
5	60	9	9; 6	10
6	75	9	9; 6	10
7	90	10.3	7; 5	13
8	60; 120	10.6	7; 6; 4	9
9	60; 120	10.6	6; 6; 6	10
10	60; 120	10.6	5; 5; 8	9
11	60; 120	10.6	4; 6; 7	9

5. Experimental results

In Fig. 4 one can see optical microscope dark field images and their calculated 2D FFT that are compared with the camera images of the three different wavelength light diffraction patterns registered on a screen. The obtained angles of diffraction were consistent with the experimental ones based on the diffraction grating equation, e.g. the angle of the first order diffraction of 1D structure presented in Fig. 4 a) was 20°, 26° and 32° for blue, green and red light lasers respectively.

From the SEM micrographs, point lattices were identified and typical lattice constants of different 2D periodic structures were determined. The SEM micrographs together with the corresponding point lattices are summarised in Fig. 5.

From the previous two beam multiple exposure experiments [48] with the same photoresist material it was known that the pattern quality depends on the ratio of the first and second exposure doses. Therefore, a set of samples (No. 8-11) with four different exposure routines were fabricated. The exposure details for these samples can be found in Table 1. The measured average absolute diffraction efficiencies of the 1st diffraction maxima, i.e. denoted as 1-6 in Fig. 4 h), and corresponding standard deviations are depicted in Fig. 6.

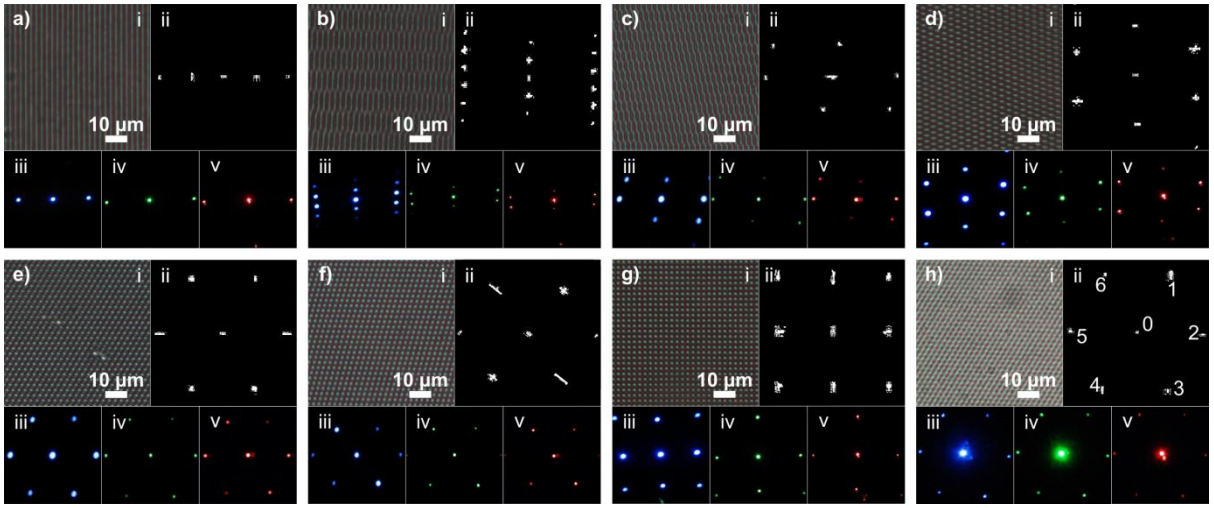

Fig. 4. Optical microscope dark field micrographs (i) of 1D (a) and 2D (b-h) structures together with their 2D FFT (ii) and camera images of diffraction patterns obtained employing different wavelength lasers: λ=405 nm (iii), λ=532 nm (iv), λ=632.8 nm (v). a) sample No. 1; b) No. 2; c) No. 3; d) No. 4; e) No. 5; f) No. 6; g) No. 7; h) No. 8. Numbers 0-6 denote diffracted beams numbering used in the diffraction efficiency measurements. Bright spots in (i) corresponds to cured area

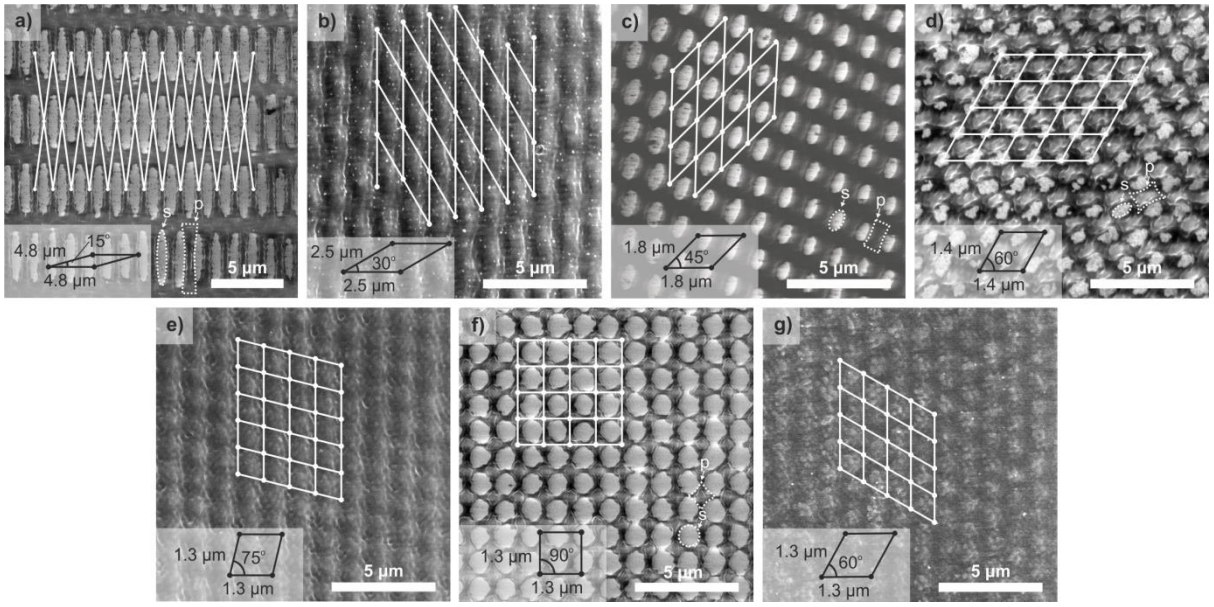

Fig. 5. SEM micrographs of different 2D periodic structures and corresponding point lattices. Mesh with the points in the cross-section of the lines were used to determine the unit cells. The insets (lower left corner) demonstrate corresponding unit cell with lattice constants a, b and γ. Areas marked with truncated lines indicate substrate ("s") and photoresist ("p"). a) sample No. 2, rhombus point lattice type, 2-fold rotational symmetry; b) No. 3, rhombus, 2-fold; c) No. 4, rhombus, 2-fold; d) No. 5, triangular, 2-fold; e) No. 6, rhombus, 2-fold; f) No. 7, square, 4-fold; g) No. 8, triangular, 6-fold

6. Discussion

Comparing Fig. 2 and Fig. 4 one can see that the simulated 1D and 2D interference pattern intensity distributions (Fig. 2 a)-h)) are in good agreement with the optical and SEM micrographs (Fig. 5) of the experimentally fabricated structures. Due to small variations in applied exposure doze and development duration (see Table 1) the obtained structures demonstrate slightly different threshold, i.e. the photoresist after development fully dissolved down to the substrate only in sample No. 2, No. 4, No. 5, No. 7 (see Fig. 5). Similar analysis of simulated interference fringes and experimentally fabricated structures has been described in [1,2,20-29,33,36-38,40,42-49]. Frequency domain images obtained from 2D FFT of the optical microscope micrographs of the structures (see Fig. 4 a)-h) inset ii) can be used for comparison with diffraction patterns of these structures (see Fig. 4 a)-h) insets iii-v), because relative distances between 0^{th} order maximum and symmetrical 1^{st} order maxima as well as corresponding angles between these maxima are the same in both images. These results

are in good agreement with [37, 49, 50] where the comparison between diffraction patterns and micrograph analysis including 2D FFT was also reported. In some cases, the longest wavelength diffraction peaks are hardly visible in the camera images because they were diffracted at higher angles than the field of view or the intensity contrast between 0^{th} and first maxima were too high for the used camera. Some of the frequency domain images demonstrate slightly elongated dots (see Fig. 4 e), f)) that could be addressed to small variations of the fabricated feature size that are visible as bright spots in the optical microscope micrographs. The structures might demonstrate different threshold due to local variations of exposure intensity or photoresist thickness variations.

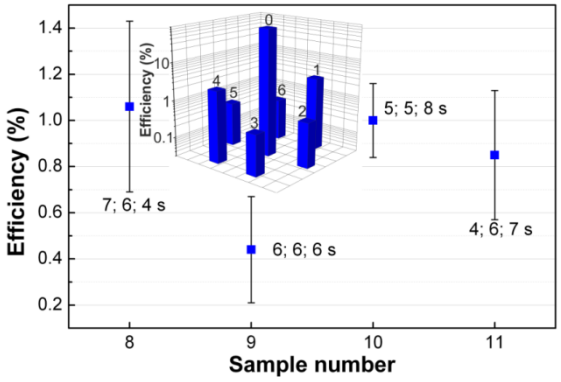

Fig. 6. Average absolute diffraction efficiencies (wavelength of illuminating laser beam: λ=405 nm) of averaged 1st diffraction maxima (Fig. 5 h) beams 1-6) of the samples No. 8-11. The numbers next to the diffraction efficiencies indicate the exposure durations of each of the three exposures with the energy density of 3.5 mW/cm^2. The inset depicts diffraction efficiencies of the sample No. 8, the numbers above the bars represent numbering of diffraction maxima identical to the ones depicted in Fig. 4 h) inset ii

It is known that the geometry of regular optical structure determines its optical responds. These 2D periodic structures can be classified employing point lattice model in terms of their regularly repeated objects in space. If every object in 2D periodic structure is imagined as a point, the corresponding array is called point lattice [51]. Any cell in the point lattice can be chosen as a unit cell, which forms point lattice by repeating itself in space. The unit cell is described by lattice constants a, b and γ. There exist five types of 2D point lattices: oblique, $a \neq b$, $\gamma \neq 90^o$; rectangular, $a \neq b$, $\gamma = 90^o$; square, $a = b$, $\gamma = 90^o$; triangular, $a = b$, $\gamma = 60^o$; and rhombus, $a = b$, $\gamma \neq 60^o$, 90^o [51]. If the structure repeats itself more than once after rotating it around certain point by 360^o, it is said that it has rotational symmetry. Then the repetitions are in $360^o/n$ angles, the structure has n-fold rotational symmetry [52]. Possible lattice types were identified from the SEM micrographs (Fig. 5). One can see that the current optical setup employed in the multiple exposure regime, when angle of rotation between the exposures was varied with a step of 15^o, provides 3 out of 5 possible point lattices types: square (Fig. 5 f)), triangular (Fig. 5 d) and g)) and rhombus (rest of the samples). It was demonstrated that the symmetry of the structures and value of angle γ can be easily controlled by choosing number of exposures and rotation angle α. In the current work most of the fabricated 2D structures have 2-fold rotational symmetry except of two, which have higher degree symmetry: 4-fold (Fig. 5 f)) and 6-fold (Fig. 5 g)). Obtained 2D lattice parameters are in good agreement with the simulated interference fringes (see Fig. 2). Other authors report the same or even higher degree experimental values of symmetry that can be reproduced employing different, more complicated HL setups: 4-fold employing two beams double exposure technique [35], 5-fold and 8-fold employing five- and eight-beam setups [25], 10-fold employing two beams and five exposures [35], 12-fold employing two beams and six exposures [22], 18-fold employing two beams and nine exposures [36], 60-fold employing three beams and ten exposures [37]. On the other hand, our system appears flexible and simple in production of a wide range of 2D structures.

Based on the previous knowledge of one [44] and two [48] exposure optimization, in the current research multiple exposure routine for the three times exposed samples was investigated and multiple exposure exposition doses were defined to develop symmetrical 1^{st} order diffraction efficiency distribution (Fig. 6). Similar experiments were described in [36] where filling factor influence on the exposure durations was investigated. The comparison of absolute diffraction efficiencies of the samples fabricated employing different exposure duration shows that the diffraction efficiency depends on the way of exposure, and the highest efficiency can be achieved when the subsequent exposure times are not equal that is in agreement with [48]. Moreover, according to our experiments the diffraction patterns produced by these structures can be used for the fast quality control of the structures – two dimensional distribution of the diffraction peaks coincides with the 2D FTT of the structures and analysis of intensities of the peaks allows one to optimize multiple exposure process.

Structure in the photoresist film demonstrated low absolute diffraction efficiency, but it is due to small height of the features. The resulting patterns can be transferred into the substrate, e.g. fused quartz, and moderately controlling the height of the pitch one can obtain efficient beam splitters of e.g. two-, four-, six-port. As it was already described elsewhere [53, 54] if one imposes the pattern of predefined height that is in the range of the wavelength in to the transparent substrate of known refractive index, e.g. fused quartz, one can obtain efficient beam splitters based on the phase shift imposed by the plane grating. In this way, employing conventional microlithography combined with dry etching and controlling the height of the structures 2-20 μm pitch efficient two-port beam splitters for spectral range from the UV to near IR [53, 54] were obtained. According to the current results, similar applications of 1D and 2D variable geometry could be easily implemented in

production of different optical devices where more sophisticated geometry is desirable.

7. Conclusions

We have shown that intensity distribution of two beam interference in multiple exposure holographic lithography can be simulated using simple approach where optical path of each beam is evaluated depending on the angular position of the sample.

We have validated this approach using two-beam multiple-exposure holographic lithography setup and demonstrated that it is suitable for high throughput and efficient fabrication method of 1D and 2D periodic structures on few cm^2 areas.

It was demonstrated that choosing number of exposures and rotation angle α structures with rhombus, triangular and square point lattice types with 2-fold, 4-fold or 6-fold rotational symmetry and angle γ can be can be obtained. The fabricated structures had a lattice constant of 1.2-4.8 μm. The diffraction patterns of these structures are well described by 2D FFT images of the optical microscope micrographs.

It was demonstrated that the diffraction patterns produced by these structures can be used for the fast quality control of the structures. Multiple exposure exposition doses were optimised and defined to develop symmetrical 1^{st} order diffraction efficiency distribution.

Acknowledgments

This research was funded by a grant (no. MIP-085/2013) from the Research Council of Lithuania. L.Š. acknowledge support by project "Promotion of Student Scientific Activities" (VP1-3.1-ŠMM-01-V-02-003) from the Research Council of Lithuania. This project is funded by the Republic of Lithuania and European Social Fund under the 2007-2013 Human Resources Development Operational Programme's priority 3. This research was performed within COST action MP1205**.**

References

[1] C. Lu, R. H. Lipson, Laser & Photonics Reviews **4**(4), 568 (2010).
[2] M. Campbell, D. N. Sharp, M. T. Harrison, R. G. Denning, A. J. Turberfield, Nature **404**, 53 (2000).
[3] A. Arriola, A. Rodriguez, N. Perez, T. Tavera, M. J. Withford, A. Fuerbach, S. M. Olaizola, Optical Materials Express **2**(11), 1571 (2012).
[4] T. Tamulevicius, R. Seperys, M. Andrulevicius, S. Tamulevicius, Photonics and Nanostructures-Fundamentals and Applications **9**(2), 140 (2011).
[5] T. Tamulevicius, R. Seperys, M. Andrulevicius, V. Kopustinskas, S. Meskinis, S. Tamulevicius, V. Mikalayeva, R. Daugelavicius, Applied Surface Science **258**(23), 9292 (2012).
[6] T. Juknius, T. Tamulevicius, I. Grazuleviciute, I. Klimiene, A. P. Matusevicius, S. Tamulevicius, Sensors and Actuators B: Chemical **204**, 799 (2014).
[7] T. Tamulevičius, R. Šeperys, M. Andrulevičius, V. Kopustinskas, Š. Meškinis, S. Tamulevičius, Thin Solid Films **519**(12), 4082 (2011).
[8] J. de Boor, N. Geyer, J. V. Wittemann, U. Gosele, V. Schmidt, Nanotechnology **21**(9), 095302 (2010).
[9] W. Lee, R. Ji, C. A. Ross, U. Gosele, K. Nielsch, Small **2**(8-9), 978 (2006).
[10] J. H. Seo, J. Park, D. Y. Zhao, H. J. Yang, W. D. Zhou, B. K. Ju, Z. Ma, IEEE Photonics Journal **5**, 6 (2013).
[11] R. Murillo, H. A. van Wolferen, L. Abelmann, J. C. Lodder, Microelectronic Engineering **78-79**, 260 (2005).
[12] N. Perez, T. Tavera, A. Rodriguez, M. Ellman, I. Ayerdi, S. M. Olaizola, Applied Surface Science **258**(23), 9370 (2012).
[13] P. Y. Baroni, B. Paivanranta, T. Scharf, W. Nakagawa, M. Roussey, M. Kuittinen, H. P. Herzig, Journal of the European Optical Society-Rapid Publications **5**, 6 (2010).
[14] S. Shaoxin, R. Xuechang, L. Shou, Y. Zhilin, Z. Yuanying, Optical Design And Engineering **52**(9), 095103 (2013).
[15] J. Aleksejeva, A. Gerbreders, M. Reinfelde, J. Teteris, J. Optoelectron. Adv. M. **13**(11-12), 1577 (2011).
[16] R. Talebzadeh, M. Soroosh, J. Optoelectron. Adv. M. **17**(11-12), 1593 (2015).
[17] T. M. Bloomstein, M. F. Marchant, S. Deneault, D. E. Hardy, M. Rothschild, Optics Express **14**(14), 6434- (2006).
[18] B. Paivanranta, A. Langner, E. Kirk, C. David, Y. Ekinci, Nanotechnology **22**(37), 375302 (2011).
[19] H. Wolferen, L. Abelmann, "Laser interference lithography," in Lithography: Principles, Processes and Materials, Nova Science Publishers, Hauppauge, NY, U.S.A., p. 113, 2011.
[20] J. de Boor, N. Geyer, U. Gosele, S. Volker, Optics Letters **34**(12), 1783 (2009).
[21] A. Rodriguez, M. Echeverria, M. Ellman, N. Perez, Y. K. Verevkin, C. S. Peng, T. Berthou, Z. Wang, I. Ayerdi, J. Savall, S. M. Olaizola, Microelectronic Engineering **86**(4-6), 937 (2009).
[22] B. Voisiat, M. Gedvilas, S. Indrisiunas, G. Raciukaitis, Journal of Laser Micro Nanoengineering **6**(3), 185 (2011).
[23] P. Prabhathan, V. M. Murukeshan, Materials, Photonic Devices, and Sensors **54**(9), 097107 (2015).
[24] R. C. Gauthier, A. Ivanov, Optics Express **12**(6), 990 (2004).
[25] A. Langner, B. Paeivaenranta, B. Terhalle, Y. Ekinci, Nanotechnology **23**(10), 105303 (2012).
[26] E. Stankevicius, M. Malinauskas, M. Gedvilas, B. Voisiat, G. Raciukaitis, Materials Science-Medziagotyra **17**(3), 244 (2011).
[27] N. D. Lai, W. P. Liang, J. H. Lin, C. C. Hsu, C. H. Lin, Optics Express **13**(23), 9605 (2005).

[28] L. Suslik, D. Pudis, J. Skriniarova, I. Martincek, I. Kubicova, J. Kovac, 18th International Vacuum Congress **32**, Ed. F. Pan, Beijing, China, 2012, p. 807.
[29] I. Byun, J. Kim, Journal of Micromechanics and Microengineering **20**(5), 055024 (2010).
[30] H. S. Jang, G. H. Kim, J. Lee, K. B. Choi, Current Applied Physics **10**(6), 1436 (2010).
[31] Q. Xie, M. H. Hong, H. L. Tan, G. X. Chen, L. P. Shi, T. C. Chong, Journal of Alloys and Compounds **449**(1-2), 261 (2008).
[32] L. Pang, W. Nakagawa, Y. Fainman, Applied Optics **42**(27), 5450 (2003).
[33] I. Mikulskas, J. Mickevicius, J. Vaitkus, R. Tomasiunas, V. Grigaliunas, V. Kopustinskas, S. Meskinis, Applied Surface Science **186**(1-4), 599 (2002).
[35] W. K. Choi, T. H. Liew, M. K. Dawood, H. I. Smith, C. V. Thompson, M. H. Hong, Nano Letters **8**(11), 3799 (2008).
[35] J. B. Yeo, S. D. Yun, N. H. Kim, H. Y. Lee, Journal of Vacuum Science & Technology B **27**(4), 1886 (2009).
[36] L. Wang, Z. H. Lu, X. F. Lin, Q. D. Chen, B. B. Xu, H. B. Sun, Journal of Lightwave Technology **31**(2), 276 (2013).
[37] N. D. Lai, J. H. Lin, D. B. Do, W. P. Liang, Y. D. Huang, T. S. Zheng, Y. Y. Huang, C. C. Hsu, "Fabrication of Two- and Three-Dimensional Photonic Crystals and Photonic Quasi-Crystals by Interference Technique" in Holography, Research and Technologies, InTech, 2011, p. 253.
[38] A. Fernandez, J. Y. Decker, S. M. Herman, D. W. Phillion, D. W. Sweeney, M. D. Perry, Journal of Vacuum Science & Technology B **15**(6), 2439 (1997).
[39] A. F. Lasagni, D. Yuan, S. Das, Advanced Engineering Materials **11**(5), 408 (2009).
[40] A. F. Lasagni, and B. S. Menéndez-Ormaza, Advanced Engineering Materials **12**, 54 (2010).
[41] C. P. Fucetola, H. Korre, K. K. Berggren, Journal of Vacuum Science & Technology B **27**(6), 2958 (2009).
[42] J. H. Moon, S. M. Yang, D. J. Pine, W. S. Chang, Applied Physics Letters **85**(18), 4184 (2004).
[43] W. D. Mao, I. Wathuthanthri, C. H. Choi, Optics Letters **36**(16), 3176 (2011).
[44] T. Tamulevicius, S. Tamulevicius, M. Andrulevicius, E. Griskonis, L. Puodziukynas, G. Janusas, A. Guobine, Experimental Techniques **32**(4), 23 (2008).
[45] T. Tamulevicius, S. Tamulevicius, M. Andrulevicius, A. Guobiene, L. Puodziukynas, G. Janusas, E. Griskonis, Materials Science-Medziagotyra **13**, 183 (2007).
[46] E. A. S. Bahaa, C. T. Malvin, Fundamentals of Photonics, Wiley, Hoboken, New Jersey, U.S.A. (2007).
[47] (2015 May 29). Processing guidelines - Positive Tone Photoresist Series ma-P 1200. Available: http://www.microresist.de/sites/default/files/download/ma-P1200_product_information.pdf
[48] T. Tamulevicius, M. Andrulevicius, A. Sileikaite, L. Puodziukynas, V. Morkunas, S. Tamulevicius, International Conference on Radiation Interaction with Materials and Its Use in Technologies 2008, Ed. A. Grigonis, Kaunas, Lithuania, 2008, p. 66-71.
[49] D. Shir, H. W. Liao, S. Jeon, D. Xiao, H. T. Johnson, G. R. Bogart, K. H. Bogart, J. A. Rogers, Nano Letters **8**(8), 2236 (2008).
[50] X. Wang, C. Y. Ng, W. Y. Tam, C. T. Chan, P. Sheng, Advanced Materials **15**(18), 1526 (2003).
[51] M. Maldovan, E. L. Thomas, Periodic Materials and Interference Lithography: for Photonics, Phononics and Mechanics, Wiley-VCH, Weinheim (2009).
[52] R. Joe, Symmetry Discovered: Concepts and Applications in Nature and Science, Dover publication, Mineloa, New York, U.S.A. (1998).
[53] T. Tamulevicius, I. Grazuleviciute, A. Jurkeviciute, S. Tamulevicius, Optics and Lasers in Engineering **51**(10), 1185 (2013).
[54] K. Jarasiunas, R. Aleksiejunas, T. Malinauskas, V. Gudelis, T. Tamulevicius, S. Tamulevicius, Review of Scientific Instruments **78**(3), 033901-1 (2007).

*Corresponding author: tomas.tamulevicius@ktu.lt